Journal of Electroanalytical Chemistry 753 (2015) 28–34

Contents lists available at ScienceDirect

Journal of Electroanalytical Chemistry

journal homepage: www.elsevier.com/locate/jelechem

The influence of acidic edge groups on the electrochemical performance of graphene nanoflakes

Mailis M. Lounasvuori, Martin Rosillo-Lopez, Christoph G. Salzmann, Daren J. Caruana, Katherine B. Holt *

Department of Chemistry, University College London, 20 Gordon St, London WC1H 0AJ, United Kingdom

ARTICLE INFO

Article history:
Received 31 October 2014
Received in revised form 30 April 2015
Accepted 9 May 2015
Available online 15 May 2015

Keywords:
Graphene
$[Fe(CN)_6]^{3-/4-}$
Oxygen-containing functionalities
pH
Isotope effect
Cyclic voltammetry
Spectroelectrochemistry
ATR-FTIR spectroscopy
Modified electrodes

ABSTRACT

Graphene nanoflakes (GNF) with lateral dimensions of ca. 30 nm and edge-terminated with carboxylic acid functionalities have been characterised and the influence of acidic functionalities on the $[Fe(CN)_6]^{3-/4-}$ redox couple studied using cyclic voltammetry and spectroelectrochemical methods. The presence of the COOH-terminated GNF in solution as well as immobilised onto an electrode surface was found to inhibit the redox reaction, supporting the conclusion that GNF promote instability of $[Fe(CN)_6]^{3-/4-}$ in solution. The redox reaction was also much less influenced by the presence of GNF in D_2O, highlighting the role played by readily available protons in destabilising the $[Fe(CN)_6]^{3-/4-}$ redox couple. In the presence of GNF in solution, an additional, very intense cyanide stretch IR band was observed that was attributed to the formation of a new, non-soluble species. When D_2O was used as the solvent, the IR spectrum showed no evidence of a new cyano species.

1. Introduction

One of the many advantages of carbon as electrode material is its relatively inert electrochemistry. However, carbon has a rich surface chemistry, and while this property is useful in that it allows the chemical modification of the electrode surface, it can also lead to unwanted oxidation in the presence of atmospheric oxygen and moisture [1,2]. The interaction of various redox species with oxygen functionalities at carbon electrodes has been investigated extensively by McCreery and coworkers [3–5]. Common redox probes can be classified roughly into three categories: those which are insensitive to surface termination (FcMeOH, $[Ru(NH_3)_6]^{3+/2+}$); those which interact with specific oxygen functionalities (such as $Fe^{3+/2+}$ with C=O) and those which are surface sensitive but apparently do not interact with specific oxygen-containing groups ($[Fe(CN)_6]^{3-/4-}$) [1].

As higher surface area nanomaterials are used, the role of carbon surface chemistry becomes increasingly important. In the past decade since it was first studied experimentally [6], graphene has attracted enormous interest in electrochemical applications owing to its large surface area and remarkable electronic properties [7–14]. Pristine graphene manufactured *via* mechanical exfoliation cannot be produced in bulk quantities. As graphene is increasingly being manufactured via reduction of graphene oxide, where an array of oxygen groups persist in the final product, the interaction of oxygen moieties with solution species will have an influence on the electrochemical response. The large variety of possible oxygen functionalities at the electrode surface makes it difficult to attribute changes in electrochemical response to specific functional groups.

Our approach to studying the influence of oxygen functionalities on the electrochemical response of graphene is to use novel graphene nanoflakes (GNF). GNF have average lateral dimensions of just 30 nm, confirmed by AFM imaging [15] with a graphene basal plane that is largely defect free. The edges of the GNF are decorated with carboxylic acid (COOH) groups, as shown by XPS and ATR-FTIR [15]. The high-resolution XPS spectrum of the C_{1s} region can be fit with two peaks: a main peak at ca. 285 eV corresponding to sp^2 carbon and a second peak at ca. 289 eV assigned to the presence of the COOH edge groups. There is no evidence for the presence of sp^3 carbon bonding, or oxygen functionalities other than COOH. Likewise, the ATR-FTIR spectrum shows a strong ν(C=O) peak at 1717 cm^{-1}, which is consistent with a carboxylic acid functionality and in good agreement with XPS data. Thus these GNF allow us to study the influence of the COOH groups on

* Corresponding author.
E-mail address: k.b.holt@ucl.ac.uk (K.B. Holt).

http://dx.doi.org/10.1016/j.jelechem.2015.05.010
1572-6657/

electrochemical response in isolation, as there are no other oxygen functionalities present. Additionally, these edge groups are present in high density and the small size of the GNF means their influence on the electrochemical performance of the flakes will be amplified.

The results presented in this paper concern the influence of the COOH edge group on the redox response of the $[Fe(CN)_6]^{3-/4-}$ couple and follow from previously reported results from our group [16]. When this redox couple was investigated using an electrode modified with COOH-terminated GNF, its voltammetric response was found to become highly irreversible as the solution pH was decreased below pH 8. At low solution pH (<6) and ionic strength the cyclic voltammetric (CV) response was very inhibited and sigmoidal in form, consistent with presence of an adsorbed blocking species at the electrode surface. When GNF terminated with amide functionalities were used instead, they were found to have no noticeable effect on this redox reaction, indicating that the COOH edge groups are responsible for the observed inhibition. Other redox probes, such as ferrocene methanol, were found to be insensitive to the identity of the GNF edge groups, so it was clear that the $[Fe(CN)_6]^{3-/4-}$ species in particular was affected by the COOH groups. Previous studies [1,4,5] have found the ET kinetics of this reaction to become slower with increasing, rather than decreasing, pH, and attributed the effect to electrostatic repulsion between COO^- functionalities at carbon electrodes and the negatively charged redox probe. In the case of COOH-GNF modified electrodes, a completely different mechanism must be responsible for the observed inhibition. The inhibition becomes observable at pH <8 and this is coincident with the pH range under which COOH-GNF are involved in complex dynamic protonation equilibria. A pH titration of GNF reported in our earlier work [16] showed a lack of a well-defined pK_a as deprotonation of the acid groups occurred over a wide pH range of ca. pH 3–8. This behaviour was attributed to different bonding environments or electrostatic/hydrogen-bonding interactions between neighbouring COOH groups. From the titration data the number of acidic protons was estimated at 7×10^{-3} mol per gram of GNF material. It appeared that the stability and reversibility of electron transfer of the $[Fe(CN)_6]^{3-/4-}$ species is strongly affected by the acidic protons of the edge groups and in this paper we describe further the role of the acidic groups on GNF in the $[Fe(CN)_6]^{3-/4-}$ electrochemistry, using in situ ATR-FTIR spectroscopy to monitor the redox reaction in both H_2O and D_2O environments.

2. Experimental

2.1. Chemicals

The GNF were prepared from multiwalled carbon nanotubes (5–20 nm outer diameter and 2–6 nm inner diameter) by chemical oxidation as reported previously [15] with some modification to the method to allow for scale-up. All other chemicals were purchased from Sigma–Aldrich and used as received. All H_2O solutions were prepared using water from a Milli-Q water purification system, with a resistivity of not less than 18.2 MΩ cm at 25 °C.

2.2. Cyclic voltammetry and electrode preparation

The experimental procedure has been reported previously [16]. CV experiments were carried out using a μ-Autolab potentiostat (Eco Chemie, NL) running GPES (v4.9) software. A boron-doped diamond (BDD) disk, 3 mm in diameter and sealed in PEEK (Windsor Scientific) was used as the working electrode, either unmodified or modified with a layer of adsorbed GNF. A coiled platinum wire served as a counter electrode. The reference electrode was Ag/AgCl (sat. KCl) (BASi, US) and all potentials are reported relative to it. The BDD electrode was polished using successively finer grades of alumina suspension down to 0.05 μm, rinsed thoroughly with ultrapure water and dried using an ambient air flow. For experiments using GNF-modified electrodes, GNF samples were drop-cast from aqueous suspensions of known concentration onto the freshly polished BDD electrode using a micropipette and allowed to dry under ambient conditions. After drying, the electrode was rinsed thoroughly with ultrapure water to remove any poorly adhered material from the surface and dried using an ambient air flow. The resulting amount of GNF on the electrode was estimated at 1.5 ± 0.5 μg in all experiments, and all CVs were recorded using a freshly modified electrode. In other experiments a known concentration of GNF was simply added to the solution along with the redox probe.

2.3. Solution-phase ATR-FTIR

2.3.1. Characterisation of GNF

Solution-phase characterisation of GNF was performed by recording mid-infrared spectra in attenuated total reflectance (ATR) mode with a Bruker Tensor 27 spectrometer (Bruker, United Kingdom) fitted with a room temperature DLaTGS detector at 4 cm^{-1} resolution and a diamond crystal as the internal reflection element. A droplet (volume ca. 50 μl) of an aqueous suspension of the GNF was applied directly onto the ATR crystal and 2 μl aliquots of 0.1 M KOH were added until the pH of the solution reached ca. 9 as determined with pH indicator paper. A spectrum was collected after each addition. Water bands were subtracted from the sample spectra by recording a background spectrum of water only prior to the experiment. The data was processed using the atmospheric compensation function of OPUS software. Changes in concentration due to the addition of aqueous aliquots of base were compensated by multiplying the spectra by the volume ratio.

2.3.2. $[Fe(CN)_6]^{3-/4-}$ stability experiments

The stability of $[Fe(CN)_6]^{3-/4-}$ in solution was investigated by recording the IR absorption of the cyanide ligands over a 24-h period. A stainless steel cell was placed on top of the IRE with two narrow steel tubes at the top of the cell that acted as the inlet and outlet for the sample. Plastic tubing was attached to the steel tubes and the sample was introduced at one end via a syringe. The sample was then pumped back and forth to remove any air bubbles. The length of the plastic tubing and the small surface area exposed to the atmosphere meant that contamination of samples in D_2O by atmospheric water was minimised. A single spectrum was computed by Fourier transformation of 250 averaged interferograms for background and sample and the software was programmed to record a spectrum every 60 min. The background spectrum was of pure water and air for experiments in H_2O and D_2O, respectively. Spectra recorded in H_2O were manipulated using the baseline and atmospheric correction functions in OPUS software. Spectra recorded in D_2O were manipulated by subtracting a spectrum of D_2O only, which was first scaled to match the absorbance at 2080–2740 cm^{-1} in sample spectra.

2.4. Spectroelectrochemical experiments

To probe the effect of solution-phase GNF on the reversibility of the $[Fe(CN)_6]^{3-/4-}$ redox couple, the IR absorption of the cyanide ligands was monitored during oxidation and reduction using an in-situ technique. ATR-FTIR spectra were recorded with a Bruker ISF 66/S spectrometer (Bruker, United Kingdom) fitted with a liquid nitrogen-cooled MCT-A detector and a silicon ATR prism at 4 cm^{-1} resolution. An electrochemical cell with a volume of 20 μl was used with a Pt mesh working electrode situated 0.1–0.3 mm

above the prism. A Pt sheet counter and Ag/AgCl reference electrode were placed in a chamber separated from the sample chamber by a Vycor frit. Working electrode potentials were set at 0 V for reduction of $[Fe(CN)_6]^{3-}$ to $[Fe(CN)_6]^{4-}$ and +350 mV for oxidation of $[Fe(CN)_6]^{4-}$ to $[Fe(CN)_6]^{3-}$. IR difference spectra were constructed by recording a background spectrum at one potential, then switching to the second potential and recording a sample spectrum at specific time intervals.

3. Results

3.1. ATR-FTIR characterisation of GNF in solution

The solution-phase IR spectra of solvated GNF are shown in Fig. 1. Initially, when only water and GNF are present and no base has been added, the pH of the solution is approximately 2 as determined with pH indicator paper. Absorption bands can be seen at 1720 cm^{-1} (C=O stretch), 1590 cm^{-1} (asymmetric COO^- stretch), 1420 cm^{-1} (symmetric COO^- stretch) and 1260 cm^{-1} (overlapping C–O stretch and O–H deformation). The GNF are partially deprotonated already before the addition of base, as indicated by the low pH of the solution and the peaks corresponding to both protonated and deprotonated forms of COOH. Adding increasing aliquots of KOH causes the signal from the C=O and C–O stretches associated with protonated carboxylic acid to decrease, whereas the two bands from COO^- gain intensity with added base. Changes can also be observed in the O–H stretch region where a decrease in absorption intensity is seen around 2900 cm^{-1} and increase around 3300 cm^{-1}. Because a background spectrum of pure water was recorded, the O–H stretch of water is subtracted from the sample spectra which initially leads to a negative feature centred at 3300 cm^{-1}. The increase in absorption at 3300 cm^{-1} upon addition of base is assigned to increased solvation of the deprotonated carboxylate groups. At the same time, the intensity of absorption around 2700 cm^{-1} decreases and this is attributed to the loss of hydrogen-bonded COOH groups. The final spectrum in Fig. 1 is recorded at pH ca. 7. Thus these in situ pH studies agree with our former observations that the flakes occupy a range of protonation states in solutions of pH 3–7.

3.2. Cyclic voltammetric studies of $[Fe(CN)_6]^{3-/4-}$ redox couple in the presence of GNF

To explore further our previous observations [16] that the $[Fe(CN)_6]^{3-/4-}$ species are unstable in the solution environment surrounding the GNF, cyclic voltammetry was performed with both $[Fe(CN)_6]^{3-}$ and GNF present in solution. All CVs were recorded at a freshly polished, clean BDD electrode. The experiment was also carried out with the $[Ru(CN)6]^{3-/4-}$ redox species in solution for comparison. It can be seen from Fig. 2 that presence of GNF in solution influences both redox reactions, but the extent to which this happens differs greatly. In the case of $[Ru(CN)_6]^{3-/4-}$, the presence of GNF in solution leads to a small increase in peak separation and a small decrease in peak height. In the case of $[Fe(CN)_6]^{3-/4-}$, on the other hand, the peak height is drastically reduced and the voltammogram has a sigmoidal shape, indicative of electrode blocking. This is the same response as we obtained when COOH-terminated GNF were immobilised directly on the electrode surface [16]. The decrease in current observed for the $[Ru(CN)6]^{3-/4-}$ couple we attribute to a small lowering of the effective diffusion coefficient of the probe due to the large GNF particles dispersed in the solution. We would expect a similar inhibition for $[Fe(CN)_6]^{3-/4-}$; however these results indicate that GNF have a profound effect on the electron transfer process of this species, rather than simply blocking diffusion. As we reported previously [16] it is specifically the COOH edge groups which affect the $[Fe(CN)_6]^{3-/4-}$ in this way, suggesting a protonation process may be responsible for these observations.

Having established the importance of the acidic functionalities in electron transfer process for $[Fe(CN)_6]^{3-/4-}$, CV experiments were carried out in low ionic strength (0.01 M KCl) solutions with GNF immobilised on the electrode surface and either H_2O or D_2O as the solvent. The results are presented in Fig. 3. When H_2O is used as the solvent, the CV shows significant inhibition in the first cycle. The response improves slightly during repeated cycling, but the 10th cycle still shows significant irreversibility of the redox reaction. In D_2O, the first cycle shows inhibited electron transfer, but the response improves during repeated cycling with increase in peak heights and decrease in peak separation. By the tenth scan, the response in D_2O is essentially reversible.

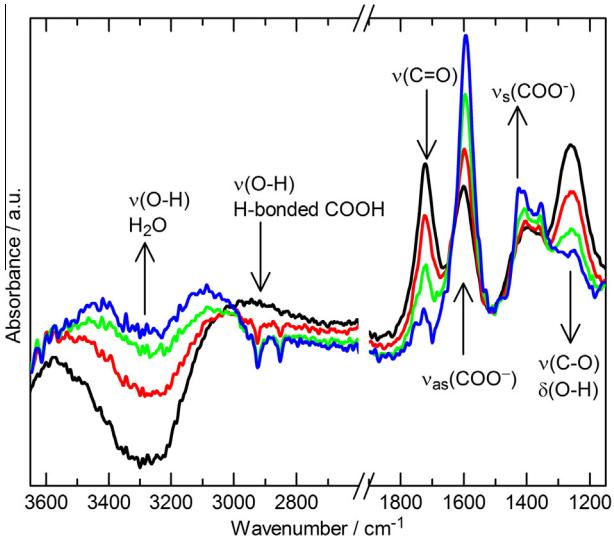

Fig. 1. Changes in IR absorption of GNF upon addition of 0.1 M KOH. GNF with no added base at pH 2 (black), pH3 (red), pH 5 (green), pH 7 (blue). (For interpretation of the references to colour in this figure legend, the reader is referred to the web version of this article.)

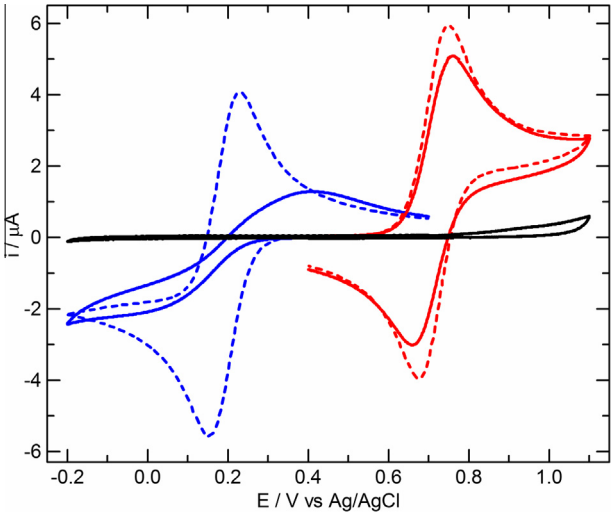

Fig. 2. CVs of GNF only (black); 0.5 mM $[Fe(CN)_6]^{3-}$ (dashed blue); 0.5 mM $[Fe(CN)_6]^{3-}$ and 34 μg ml^{-1} GNF (solid blue); 0.5 mM $[Ru(CN)_6]^{4-}$ (dashed red); 0.5 mM $[Ru(CN)_6]^{4-}$ and 34 μg ml^{-1} GNF (solid red). Electrolyte: 0.01 M KCl. Scan rate: 50 mV s^{-1}. (For interpretation of the references to colour in this figure legend, the reader is referred to the web version of this article.)

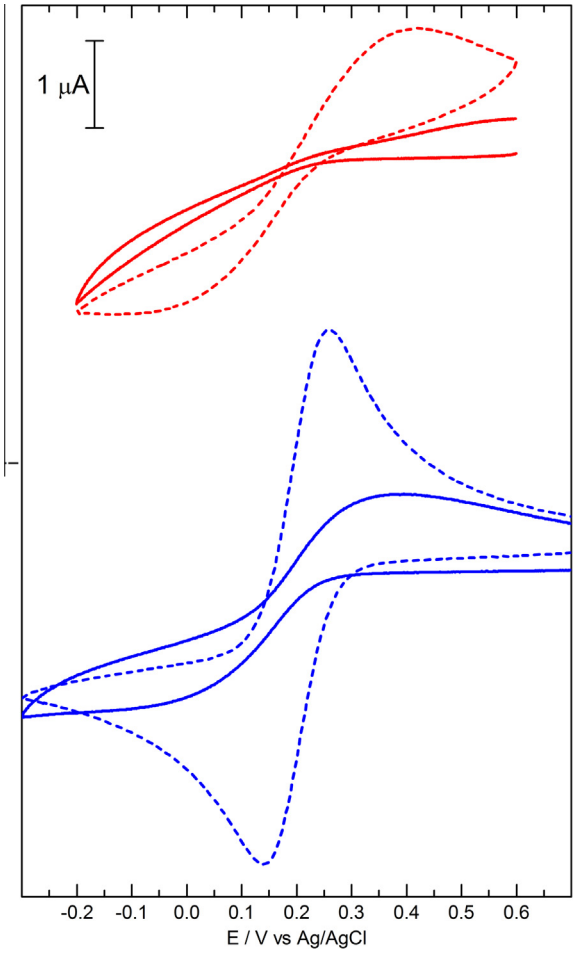

Fig. 3. CVs of 0.5 mM $K_3[Fe(CN)_6]$ in 0.01 M KCl in H_2O (red) and D_2O (blue). First scans (solid lines) and 10th scans (dashed lines) shown. Scan rate: 50 mV s^{-1}. (For interpretation of the references to colour in this figure legend, the reader is referred to the web version of this article.)

When the GNF are surrounded with H_2O molecules, the constant protonation and deprotonation of the carboxylic acid edge groups does not lead to a change in the chemical identity of the acid groups. However, if the H_2O molecules are replaced by D_2O, the dynamic acid–base equilibrium will gradually lead to predominantly COOD around the flake edges as the protons are exchanged and diffuse away from the electrode surface. Therefore we propose that during the first cycles in D_2O, the GNF edges are still mostly decorated with COOH groups and these inhibit the redox reaction. However, as COOD groups begin to dominate, the redox reaction is allowed to proceed uninhibited, leading to a near reversible CV by the 10th scan. The results also suggest that if an electrode blocking species is responsible for the inhibited electron transfer, it forms reversibly and can dissolve or desorb from the electrode surface according to changes in the diffusion layer. Thus the redox reaction is able to become more reversible with cycling in D_2O as the concentration of protons at the GNF-modified electrode surface decreases.

3.3. Spectroelectrochemistry of $[Fe(CN)_6]^{3-/4-}$

The $[Fe(CN)_6]^{3-/4-}$ redox reaction can be conveniently monitored with ATR-FTIR because the cyanide stretch is sensitive to the oxidation state of the iron centre. $[Fe(CN)_6]^{3-}$ absorbs at 2116 cm^{-1}, whereas in $[Fe(CN)_6]^{4-}$ the absorption frequency is shifted to 2036 cm^{-1} and the extinction coefficient is four times larger. ATR-FTIR coupled with in-situ controlled potential experiments were performed for 1 mM $K_3[Fe(CN)_6]$ in 0.01 M KCl. The sample was introduced to the in situ electrochemical cell and a potential of 0 V was applied to drive the reduction of $[Fe(CN)_6]^{3-}$ to $[Fe(CN)_6]^{4-}$. The resulting IR spectrum shows a negative $[Fe(CN)_6]^{3-}$ band and positive $[Fe(CN)_6]^{4-}$ band (solid line, Fig. 4a). When the intensity of the $[Fe(CN)_6]^{4-}$ band did not increase anymore, all $[Fe(CN)_6]^{3-}$ present in the sample chamber was assumed to have been converted to $[Fe(CN)_6]^{4-}$. The reaction reached completion in about 2 min, as indicated by the intensity of the $[Fe(CN)_6]^{4-}$ band. The height of the $[Fe(CN)_6]^{4-}$ band as a function of time is plotted in Fig. 4b.The potential was then switched to +350 mV to oxidise $[Fe(CN)_6]^{4-}$ back to $[Fe(CN)_6]^{3-}$. The resulting IR spectrum shows a positive $[Fe(CN)_6]^{3-}$ band and negative $[Fe(CN)_6]^{4-}$ band (dashed line, Fig. 4a). As was the case for the reduction, the negative $[Fe(CN)_6]^{4-}$ band reached full height after about 2 min, indicating full conversion back to $[Fe(CN)_6]^{3-}$. The $[Fe(CN)_6]^{3-}$ solution was then replaced by a solution containing 1 mM $K_3[Fe(CN)_6]$ in 0.01 M KCl and 3.2 μg ml^{-1} of GNF. The concentration of acidic protons from the GNF is estimated to be 22 μM and only a small fraction would be dissociated. Therefore the GNF did not significantly alter the pH of the solution. The experiment was then repeated and a potential of 0 V applied. With the GNF present, the reaction proceeded much more slowly. After 2 min, the $[Fe(CN)_6]^{4-}$ band was only 40% of the intensity expected for full conversion of $[Fe(CN)_6]^{3-}$ to $[Fe(CN)_6]^{4-}$. Full conversion took approximately 9 min, compared to 2 min for the same volume and concentration of the control solution. The influence of GNF on the oxidation reaction was essentially the same.

The observations reported here support the CV experiments described in Section 3.2. The presence of GNF clearly inhibits the reversibility of the $[Fe(CN)_6]^{3-/4-}$ redox couple. Moreover, it was shown in Fig. 2 that the observed decrease in current could not be explained by diffusion effects alone. Therefore, the reason why the reaction takes longer to complete with GNF in solution is likely to lie in the solution stability of the redox species.

3.4. Monitoring the stability of $[Fe(CN)_6]^{3-/4-}$ with ATR-FTIR

Beriet and Pletcher [17] made the observation that the poisoning of an electrode surface by the $[Fe(CN)_6]^{3-/4-}$ redox couple required the presence of both Fe(II) and Fe(III) species. We therefore used an equimolar solution of $K_3[Fe(CN)_6]$ and $K_4[Fe(CN)_6]$ in H_2O to probe their stability in solution in the absence of applied potential. To gauge the impact of GNF on the stability of $[Fe(CN)_6]^{3-/4-}$, a second solution was prepared, this one also containing 30 μg ml^{-1} GNF. The concentration of GNF was high enough to impart a brownish hue to the solution but low enough to not alter the pH significantly (pH of both solutions 6.5 ± 0.1).

The IR spectrum of both samples initially shows two peaks; the $[Fe(CN)_6]^{4-}$ CN stretch at 2036 cm^{-1} and the $[Fe(CN)_6]^{3-}$ CN stretch at 2116 cm^{-1} (Fig. 5). No peaks are detected in the 1700–1200 cm^{-1} region that could be associated with GNF, although the concentration of flakes is too low for this purpose. Over time, a third peak begins to emerge in both samples. In the control solution, this peak at 2069 cm^{-1} is detectable above the noise after about 13 h, whereas with GNF in solution, the intensity of this third peak surpasses that of the $[Fe(CN)_6]^{3-}$ peak after 3 h. Mixing the GNF sample by pumping gently with a syringe back and forth caused a decrease in the intensity of the peak at 2069 cm^{-1}.

The new band is very high in intensity compared to the other two CN stretch bands. Given that the $[Fe(CN)_6]^{4-}$ and $[Fe(CN)_6]^{3-}$ bands are not greatly diminished, it is clear that the new cyano species cannot be present in high concentration. The intensity of the new band may then be due to either a species present in low concentration with a high extinction coefficient, or the accumulation of a species in the region near the ATR prism. A new species

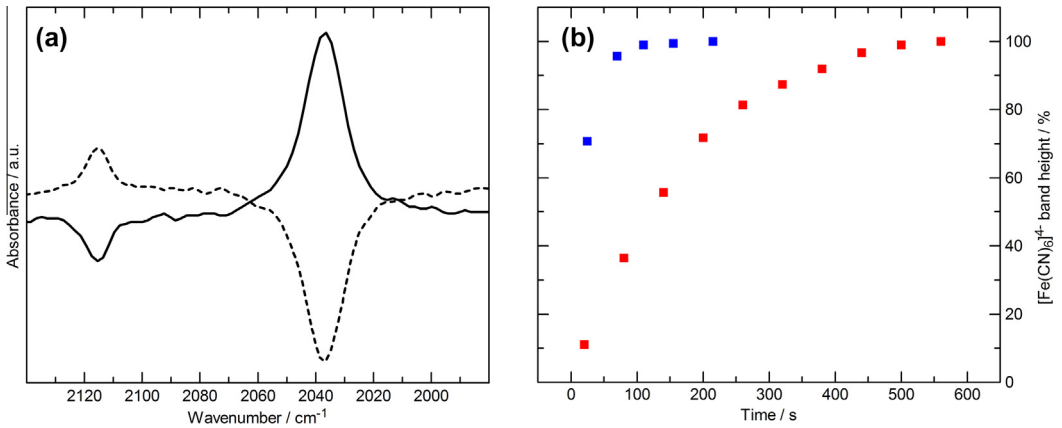

Fig. 4. (a) Difference spectra of $[Fe(CN)_6]^{3-}$ and $[Fe(CN)_6]^{4-}$. After reduction of $K_3[Fe(CN)_6]$, the IR spectra show a negative $[Fe(CN)_6]^{3-}$ band and positive $[Fe(CN)_6]^{4-}$ band (solid line). Oxidation of $[Fe(CN)_6]^{4-}$ results in a positive $[Fe(CN)_6]^{3-}$ band and negative $[Fe(CN)_6]^{4-}$ band (dashed line). (b) Height of the $[Fe(CN)_6]^{4-}$ CN stretch band at 2036 cm^{-1} relative to the intensity of absorption at full conversion as a function of time. Blue squares: 1 mM $K_3[Fe(CN)_6]$; red squares: 1 mM $K_3[Fe(CN)_6]$ and 3.2 μg ml^{-1} of GNF. Electrolyte: 0.01 M KCl. Potentials: 0 V (reduction), +350 mV (oxidation). (For interpretation of the references to colour in this figure legend, the reader is referred to the web version of this article.)

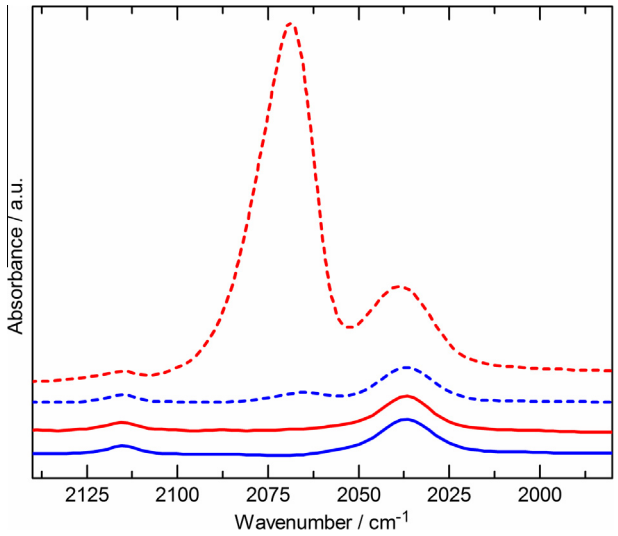

Fig. 5. 2 mM $K_3[Fe(CN)_6]$ and 2 mM $K_4[Fe(CN)_6]$ in H_2O at $t = 0$ h (solid blue) and at $t = 24$ h (dashed blue); with 30 μg ml^{-1} GNF at $t = 0$ h (solid red) and at $t = 24$ h (dashed red). (For interpretation of the references to colour in this figure legend, the reader is referred to the web version of this article.)

with a high extinction coefficient is unlikely, as the most plausible solution species candidate that absorbs in this region is free cyanide, the absorption coefficient of which is very small compared to the bound form [18]. The most likely explanation is the accumulation of a non-soluble species at the surface of the internal reflection element, which in the cell geometry is at the bottom of the cell. This would also explain why the intensity of the other CN stretch bands does not change significantly, since the amount of precipitate does not need to be large in order to give an appreciable signal. UV–Vis spectra taken in situ with the same solution (not shown) do not offer evidence of the formation of a coloured species, but it is important to bear in mind that the UV–Vis probes the bulk solution (where the overall concentration of this new species is low) whereas ATR-FTIR only reaches a few microns at the bottom of the cell (where the species accumulates).

As described in Section 3.2, the identity of solvent has a marked influence on the reversibility of the $[Fe(CN)_6]^{3-/4-}$ redox couple. To further explore this, stability experiments were repeated in D_2O as shown in Fig. 6. In H_2O, a new band appeared in between the two cyanide stretch bands after a couple of hours. In D_2O, no new band is seen after four hours whereas in H_2O, the new band at that point was already comparable in size to the $[Fe(CN)_6]^{4-}$ stretch. After 24 h in D_2O the new band did become evident, but its appearance is accompanied with a H_2O band due to H_2O contamination from atmospheric moisture, leading to the conclusion that the presence of appreciable concentration of protons is necessary for the decomposition/precipitation reaction to proceed.

4. Discussion

Above, we have described how the presence of GNF influences the $[Fe(CN)_6]^{3-/4-}$ redox system. In our previous work [16] it was determined that it is specifically the acidic groups around the edges of GNF that are responsible for the irreversible behaviour of the $[Fe(CN)_6]^{3-/4-}$ redox couple. Here, we have explored further the influence of protons on this redox reaction. The reversibility and electron transfer rate of the $[Fe(CN)_6]^{3-/4-}$ redox system has been shown by others to also depend on the concentration and identity of cations in solution [17,19]. Peter et al. have suggested

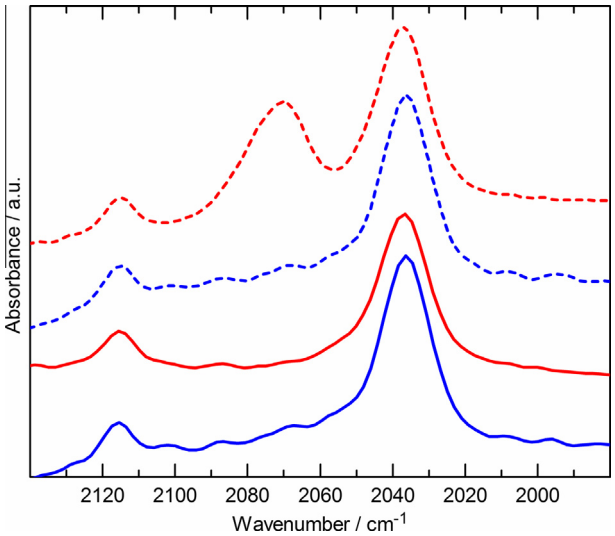

Fig. 6. ATR-FTIR spectra of 2 mM $K_3[Fe(CN)_6]$ and 2 mM $K_4[Fe(CN)_6]$ with 30 μg ml^{-1} GNF In H_2O at $t = 0$ h (solid red) and $t = 4$ h (dashed red), in D_2O at $t = 0$ h (solid blue) and $t = 4$ h (dashed blue). (For interpretation of the references to colour in this figure legend, the reader is referred to the web version of this article.)

that the rate of electron transfer depends on the concentration of an activated species containing one or more cations, and that electron transfer is considerably lower in the absence of ion-pairing, for example in electrolyte solutions of low ionic strength [19]. Additionally, it is known that $[Fe(CN)_6]^{3-/4-}$ can be unstable in solution of low ionic strength and low pH, and cyanide ligand loss and subsequent decomposition and adsorption onto electrodes have been observed by several groups [17,20–25]. Protonation and decomposition of $[Fe(CN)_6]^{3-}$ have been observed to occur simultaneously [26], and although our sample solutions at pH 6 would not be considered acidic enough to cause decomposition of $[Fe(CN)_6]^{3-}$, the high density of COOH groups on the GNF may lead to localised acidic conditions, promoted by the ready availability of protons at the edges of the flakes. Thus there are several mechanisms by which the very acidic local environment of the COOH-GNF could inhibit electron transfer, including disruption to the ion paired activated species required for fast electron transfer, protonation of CN ligands, loss of ligands or formation of insoluble decomposition products.

When deuterated water is substituted for H_2O, the presence of GNF has much less influence on the $[Fe(CN)_6]^{3-/4-}$ redox reaction. Consecutive cycles in D_2O saw the voltammetric response of $[Fe(CN)_6]^{3-/4-}$ quickly return to near reversible. ATR IR also showed the $[Fe(CN)_6]^{3-/4-}$ species to be more stable in the presence of GNF when dissolved in D_2O rather than H_2O. The substitution of deuterium for hydrogen in a water molecule has little effect on the molecular dimensions defined by bond length and bond angle, but the O–D bond is slightly stronger than the O–H bond. The difference in bond strength leads to a smaller dissociation constant for D_2O than H_2O, making H_2O a fivefold stronger acid [27]. Liquid D_2O is more viscous than liquid H_2O and has a slower rate of molecular reorientations and translations [28], leading to the conclusion that there is more structural order in D_2O due to a higher degree of hydrogen bonding [29]. This can be attributed to lower intermolecular vibrational frequencies caused by isotopic substitution but also the greater strength of hydrogen bonding in D_2O than in H_2O [29]. Additionally, protons are able to diffuse rapidly in water *via* the Grotthuss mechanism [30]. It has recently been demonstrated that the mechanism is strongly influenced by the local hydration structure of the proton and involves the concerted motion of several protons [31]. The reorganisation and rotation of molecules involved in the Grotthuss mechanism are slower in D_2O than in H_2O, making heavy water less efficient in proton transport. Thus the instability of $[Fe(CN)_6]^{3-/4-}$ in the presence of GNF appears to be exacerbated by the readily available H^+ in the localised acidic conditions in the region of the carboxylic acid edge groups. Increased stability in D_2O can be attributed either to the increased strength of the O–D bond (making D^+ less available) or slower diffusion of D^+ from the GNF to $[Fe(CN)_6]^{3-/4-}$.

The results described in Section 3.4 lead to the interpretation that the presence of GNF in an aqueous solution of $K_3[Fe(CN)_6]$ and $K_4[Fe(CN)_6]$ promotes the decomposition of $[Fe(CN)_6]^{3-}$ and/or $[Fe(CN)_6]^{4-}$. The intense new IR absorption band that emerges after only some hours indicates the formation of a non-soluble species. The best-known hexacyanoferrate complex is Prussian Blue, which absorbs in the region of 2070–2100 cm^{-1} depending on the whether the Fe^{3+} is hydrolysed (lower cm^{-1}) or not (higher cm^{-1}) [32] and it could be envisaged to accumulate at the bottom of the cell by precipitation, although the UV–Vis data does not offer direct evidence of Prussian Blue. Other well-known related compounds are Prussian White (all ferrous), which absorbs between 2080–2060 cm^{-1} and Prussian Yellow/Everitt's Salt (all ferric), absorbing near 2175 cm^{-1}. During the reduction of $[Fe(CN)_6]^{3-}$ to $[Fe(CN)_6]^{4-}$ an adsorbed intermediate has been reported that absorbs between 2070–2080 cm^{-1} [33]. Similarly, an adsorbed species on Pt has been observed during potential cycling that gives an IR band 2090–2070 cm^{-1} and inhibits ET, concluded to be a (unnamed) colourless soluble (i.e. containing K^+) mixed-valency compound [24]. Hence although we have clearly detected a decomposition product formed in the presence of COOH-terminated GNF we cannot be absolutely certain of its identity.

5. Conclusions and future work

COOH-terminated GNF have been used to probe the influence of acidic functionalities on the $[Fe(CN)_6]^{3-/4-}$ redox couple by cyclic voltammetry and controlled-potential experiments with in-situ ATR-FTIR. The redox reaction is severely inhibited by the presence of the GNF in solution as well as at the electrode surface, supporting the conclusion that GNF promote instability of $[Fe(CN)_6]^{3-/4-}$ in solution. The formation of a precipitate from solutions of $[Fe(CN)_6]^{3-}$ and $[Fe(CN)_6]^{4-}$ in the presence of GNF was concluded from ATR-FTIR spectroscopy. The precipitate did not form when D_2O was used as the solvent. GNF had much less influence on the redox reaction in D_2O, highlighting the role played by readily available protons at the flake edge.

We have suggested here that the instability of $[Fe(CN)_6]^{3-/4-}$ may be caused by protonation and subsequent decomposition of the complex anion. Work is under way to monitor this process and the protonation state and H^+/D^+ exchange of the carboxylic acid edge groups around GNF dissolved in D_2O with ^1H NMR. At a given temperature, D_2O is more structured than H_2O, hence substituting D_2O for H_2O is therefore comparable to lowering the temperature of the solution. Therefore it would be interesting to see if there is a temperature dependence of the CV response of $[Fe(CN)_6]^{3-/4-}$ in H_2O when GNF are present. Other solvents will also be used to study the influence of GNF on the reversibility and stability of this redox couple.

Understanding the role of different oxygen-containing functional groups on the electrochemical performance of graphene materials is essential in determining the importance of defect chemistry when it is used as an electrode. Here we have been able to study the influence of COOH groups in isolation as our well-characterised flakes are shown to contain no other functionalities. By changing the GNF terminations we aim to study the effect of other edge groups on the electrochemical response of graphene.

Conflict of interest

The authors confirm that there is no conflict of interest.

Acknowledgments

We thank EPSRC/UCL Chemistry Department for studentship for Mailis Lounasvuori and Martin Rosillo-Lopez. Christoph Salzmann thanks the Royal Society for the award of a URF. The work was funded partly by EPSRC grant EP/J010006/1. ATR-FTIR experiments using the Bruker ISF 66/S spectrometer were performed at the Glynn Laboratory, UCL. The help and advice by Prof Peter R. Rich and his group is gratefully acknowledged.

References

[1] R.L. McCreery, Advanced carbon electrode materials for molecular electrochemistry, Chem. Rev. 108 (2008) 2646–2687.
[2] G.G. Wildgoose, P. Abiman, R.G. Compton, Characterising chemical functionality on carbon surfaces, J. Mater. Chem. 19 (2009) 4875–4886.
[3] C.A. McDermott, K.R. Kneten, R.L. McCreery, Electron transfer kinetics of aquated $Fe^{+3/+2}$, $Eu^{+3/+2}$, and $V^{+3/+2}$ at carbon electrodes: inner sphere catalysis by surface oxides, J. Electrochem. Soc. 140 (1993) 2593–2599.
[4] P. Chen, M.A. Fryling, R.L. McCreery, Electron transfer kinetics at modified carbon electrode surfaces: the role of specific surface sites, Anal. Chem. 67 (1995) 3115–3122.

[5] P. Chen, R.L. McCreery, Control of electron transfer kinetics at glassy carbon electrodes by specific surface modification, Anal. Chem. 68 (1996) 3958–3965.
[6] K.S. Novoselov, A.K. Geim, S.V. Morozov, D. Jiang, Y. Zhang, S.V. Dubonos, I.V. Grigorieva, A.A. Firsov, Electric field effect in atomically thin carbon films, Science 306 (2004) 666–669.
[7] N.G. Shang, P. Papakonstantinou, M. McMullan, M. Chu, A. Stamboulis, A. Potenza, S.S. Dhesi, H. Marchetto, Catalyst-free efficient growth, orientation and biosensing properties of multilayer graphene nanoflake films with sharp edge planes, Adv. Funct. Mater. 18 (2008) 3506–3514.
[8] D.A.C. Brownson, C.E. Banks, CVD graphene electrochemistry: the role of graphitic islands, PCCP 13 (2011) 15825–15828.
[9] W. Li, C. Tan, M.A. Lowe, H.D. Abruña, D.C. Ralph, Electrochemistry of individual monolayer graphene sheets, ACS Nano 5 (2011) 2264–2270.
[10] A.T. Valota, I.A. Kinloch, K.S. Novoselov, C. Casiraghi, A. Eckmann, E.W. Hill, R.A.W. Dryfe, Electrochemical behavior of monolayer and bilayer graphene, ACS Nano 5 (2011) 8809–8815.
[11] C. Tan, J. Rodríguez-López, J.J. Parks, N.L. Ritzert, D.C. Ralph, H.D. Abruña, Reactivity of monolayer chemical vapor deposited graphene imperfections studied using scanning electrochemical microscopy, ACS Nano 6 (2012) 3070–3079.
[12] E. Kibena, M. Mooste, J. Kozlova, M. Marandi, V. Sammelselg, K. Tammeveski, Surface and electrochemical characterisation of CVD grown graphene sheets, Electrochem. Commun. 35 (2013) 26–29.
[13] N.L. Ritzert, J. Rodríguez-López, C. Tan, H.D. Abruña, Kinetics of interfacial electron transfer at single-layer graphene electrodes in aqueous and nonaqueous solutions, Langmuir 29 (2013) 1683–1694.
[14] M. Velický, D.F. Bradley, A.J. Cooper, E.W. Hill, I.A. Kinloch, A. Mishchenko, K.S. Novoselov, H.V. Patten, P.S. Toth, A.T. Valota, S.D. Worrall, R.A.W. Dryfe, Electron transfer kinetics on mono- and multilayer graphene, ACS Nano 8 (2014) 10089–10100.
[15] C.G. Salzmann, V. Nicolosi, M.L.H. Green, Edge-carboxylated graphene nanoflakes from nitric acid oxidised arc-discharge material, J. Mater. Chem. 20 (2010) 314–319.
[16] M.M. Lounasvuori, M. Rosillo-Lopez, C.G. Salzmann, D.J. Caruana, K.B. Holt, Electrochemical characterisation of graphene nanoflakes with functionalised edges, Faraday Discuss. 172 (2014) 293–310.
[17] C. Beriet, D. Pletcher, A microelectrode study of the mechanism and kinetics of the ferro/ferricyanide couple in aqueous media: the influence of the electrolyte and its concentration, J. Electroanal. Chem. 361 (1993) 93–101.
[18] S. Le Caër, G. Vigneron, J.P. Renault, S. Pommeret, First coupling between a LINAC and FT-IR spectroscopy: the aqueous ferrocyanide system, Chem. Phys. Lett. 426 (2006) 71–76.
[19] L.M. Peter, W. Dürr, P. Bindra, H. Gerischer, The influence of alkali metal cations on the rate of the $Fe(CN)_6^{4-}/Fe(CN)_6^{3-}$ electrode process, J. Electroanal. Chem. 71 (1976) 31–50.
[20] A. Więckowski, M. Szklarzyk, The state of the polycrystalline platinum electrode during the heterogeneous electron-transfer reaction: $Fe(CN)_6^{3-}+eFe(CN)_6^{4-}$, J. Electroanal. Chem. 142 (1982) 157–170.
[21] S. Pons, M. Datta, J.F. McAleer, A.S. Hinman, Infrared spectroelectrochemistry of the $Fe(CN)_6^{4-}/Fe(CN)_6^{3-}$ redox system, J. Electroanal. Chem. 160 (1984) 369–376.
[22] J. Kawiak, P.J. Kulesza, Z. Galus, A search for conditions permitting model behavior of the $Fe(CN)^{3-}/_6^{4-}$ system, J. Electroanal. Chem. 226 (1987) 305–314.
[23] C. Lee, F.C. Anson, Inhibition of the electroreduction of $Fe(CN)_6^{3-}$ at microelectrodes in the absence of supporting electrolyte: mediation of the inhibited reduction by methyl viologen, J. Electroanal. Chem. 323 (1992) 381–389.
[24] C.M. Pharr, P.R. Griffiths, Infrared spectroelectrochemical analysis of adsorbed hexacyanoferrate species formed during potential cycling in the ferrocyanide/ferricyanide redox couple, Anal. Chem. 69 (1997) 4673–4679.
[25] A.A. Karyakin, Prussian blue and its analogues: electrochemistry and analytical applications, Electroanalysis 13 (2001) 813–819.
[26] P.L. Domingo, B. García, J.M. Leal, Acid–base behaviour of the ferricyanide ion in perchloric acid media. Spectrophotometric and kinetic study, Can. J. Chem. 68 (1990) 228–235.
[27] T. Riley, F.A. Long, Deuterium isotope and solvent effects on the kinetics of the keto-enol interconversion of 2-acetylcyclohexanone, J. Am. Chem. Soc. 84 (1962) 522–526.
[28] S.N. Vinogradov, R.H. Linnell, Hydrogen bonding, Van Nostrand Reinhold, New York; London, 1971.
[29] G. Némethy, H.A. Scheraga, Structure of water and hydrophobic bonding in proteins. IV. The thermodynamic properties of liquid deuterium oxide, J. Chem. Phys. 41 (1964) 680–689.
[30] C.J.T. de Grotthuss, Memoir on the decomposition of water and of the bodies that it holds in solution by means of galvanic electricity, Biochim. Biophys. Acta (BBA) – Bioenerg. 1757 (2006) 871–875.
[31] A. Hassanali, F. Giberti, J. Cuny, T.D. Kühne, M. Parrinello, Proton transfer through the water gossamer, Proc. Natl. Acad. Sci. 110 (2013) 13723–13728.
[32] P.A. Christensen, A. Hamnett, S.J. Higgins, A study of electrochemically grown Prussian blue films using Fourier-transform infra-red spectroscopy, J. Chem. Soc., Dalton Trans. (1990) 2233–2238.
[33] K. Kunimatsu, Y. Shigematsu, K. Uosaki, H. Kita, Study of the $Fe(CN)_6^{3-}/Fe(CN)_6^{4-}$ redox system on Pt by EMIRS: Part I. infrared spectra of the intermediates in the charge transfer, J. Electroanal. Chem. 262 (1989) 195–209.